

Through-the-sensor sharpness estimation for synthetic aperture sonar images

1st Marc Geilhufe

Norwegian Defence Research Establishment (FFI)
Kjeller, Norway
marc.geilhufe@ffi.no

2nd Roy Edgar Hansen

Norwegian Defence Research Establishment (FFI)
Kjeller, Norway
roy-edgar.hansen@ffi.no

3rd Øivind Midtgaard

Norwegian Defence Research Establishment (FFI)
Kjeller, Norway
oivind.midtgaard@ffi.no

4th Stig Asle Vaksvik Synnes

Norwegian Defence Research Establishment (FFI)
Kjeller, Norway
stig-asle.synnes@ffi.no

Abstract—Synthetic aperture sonar (SAS) is emerging as the reference technique for high resolution imaging of the seabed. Given the insufficient positioning accuracy, the harsh ocean environment and lack of stability on relatively small platforms carrying the sonar, an optimal SAS image quality is not always guaranteed. In this paper, we present a technique to quantify the image quality based on the actual SAS images through-the-sensor. We have previously presented approaches to predict the sharpness in SAS images from meta-data, but in practice those have not always been precise given their predictive nature. We now introduce an image-based sharpness estimate that can be combined with the meta-data prediction. The image-based estimate is derived by locating candidate point scatterers and estimating key parameters from their point-spread functions. These provide information about defocus and unwanted grating lobes, the two most common types of image degradation in SAS. This technique requires texture in the image. For areas where no point scatterers can be detected, we rely only on meta-data to predict sharpness.

Index Terms—Synthetic aperture sonar, performance estimation, image quality, sharpness

I. INTRODUCTION

With the emergence and technical developments of Autonomous Underwater Vehicles (AUVs) over the last two decades, these platforms have proven to be a valuable asset for many applications, including mine countermeasure (MCM) operations. AUVs equipped with high-resolution synthetic aperture sonar (SAS) provide a superior combination of data quality and sensor range.

At FFI, we have worked on through-the-sensor performance estimation methods over the last years and derived a model for the sonar mine search phase performance based on a number of parameters given a priori and measured in-situ [1]. The two main parameters are: Image quality to quantify the performance of the sonar in the given environment [2]; Image complexity to quantify the difficulty of detecting and classifying a target against the given image background [3]. Both parameters depend on various sub-parameters. For image quality, these are:

- Generalized signal to noise ratio (SNR), which is an estimate of the SNR in the actual measured sonar data at a given location in the image. It can be estimated reliably from the side-scan interferometric coherence, if two receiver arrays are available for each side of the vehicle [4].
- Radiometric resolution representing the pixel value accuracy or target strength accuracy. The pixel value carries valuable information, and is strongly utilized in synthetic aperture radar (SAR) [5]. It requires absolute calibrated hardware and software, and proper treatment of geometry. Currently, we do not utilize this, and assume this parameter to be constant.
- Theoretical geometric resolution of the SAS system, which is a constant for given hardware and processing choices.
- Sharpness, which is an estimate of how well focused a SAS image is. It describes how close the actual resolution is to the theoretical (maximum possible) geometric resolution.

Other through-the-sensor quality estimates could provide valuable information, e.g. shadow contrast [6] as an additional means for assessing the impact from grating lobes.

In this paper, we concentrate on quantifying the sharpness in SAS images through-the-sensor based on the actual images themselves. We first locate candidate point scatterers and then measure their point spread function (PSF) properties [7, chapter 4], inspired by the approach suggested in [8].

We first discuss the limiting factors for SAS image quality and then describe a technique to estimate image sharpness from meta-data and directly from the image. We apply the technique on example data from the HISAS 1032 interferometric SAS on-board a HUGIN AUV and evaluate the accuracy of the estimated sharpness values on good and degraded images.

II. SAS IMAGE QUALITY

There are several common causes for reduced SAS image quality [9], which we list below along with information on how each cause impacts our work:

- 1) *Unwanted multiple reflections from the sea surface in shallow waters:* We use interferometric coherence as a measure of this impact on SAS image quality [4]. We thereby have an accurate tool to measure the reduced quality due to multipath.
- 2) *Ocean currents causing the AUV to run with horizontal crab:* There are different signal processing strategies that may handle crab well or poorly. The output image quality is therefore a function of choice of algorithm.
- 3) *Rough terrain causing vertically nonlinear tracks:* It becomes more demanding to produce a perfectly sharp image when the sensor moves in rough terrain.
- 4) *Guidance and control induced nonlinear tracks:* Any deviation from a straight line, either in the horizontal or vertical plane, will cause less favorable conditions for successful SAS processing.
- 5) *Unknown and uncompensated navigational errors:* We use an integrated navigation solution based both on the inertial navigation and sonar micro-navigation. Any error in the micro-navigation (e.g. loss of track due to multipath) will therefore also affect the navigation solution.
- 6) *Sound speed errors:* The sound speed in the ocean varies up to 4% with depth and season. SAS is nearfield imaging, and incorrect sound speed will cause defocus.

These six common causes for potential reduction of SAS image quality should be treated differently. 1) is a fundamental limitation. If the sonar data are contaminated with unwanted multipath, there basically does not exist any good solution to correct that problem. For 2) - 4), there may be alternative processing strategies that will improve the SAS image quality. In 5), the error is unknown, and therefore harder to categorize. 6) is typically slowly varying, relatively easy to monitor, and relatively easy to correct for.

We suggest a two-fold approach for determining the reduced sharpness in SAS images both using meta-data and extracting information from the images (see Fig. 1). Relevant factors for the meta-data based prediction are described in [2]. Over the years, we have found the most important meta-data contributions are to handle both horizontal (yaw) and vertical (pitch) vehicle crab, deviation from a straight vehicle track and micro-navigation coherence. The meta-data based prediction will not be described further in this article since the main scope here is to present our image-based contribution to sharpness estimation. In all cases mentioned above, except 1), any predicted sharpness cannot fully replace a direct image-based estimated sharpness.

Our image-based method requires texture in the image. If there is not sufficient texture present, we solely use the meta-data prediction that has been our standard sharpness estimator up to date.

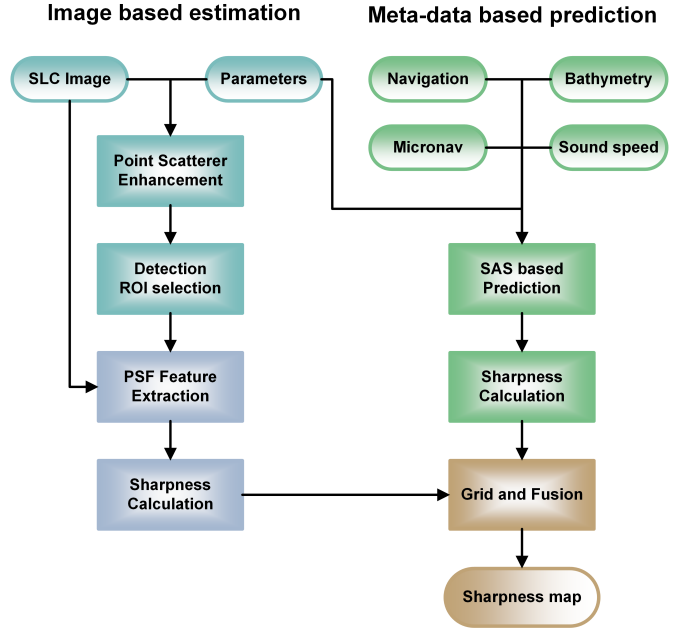


Fig. 1. Sharpness estimation flowchart

III. SHARPNESS ESTIMATION

Sharpness describes how close the actual resolution is to the theoretical geometric resolution. When these two resolutions deviate consistently from each other for nearby point scatterers, we have an indication for image degradation. This is the basis for constructing our image-based sharpness estimation, which consists of several steps visualized in the left side of Fig. 1.

Starting from a single look complex (SLC) SAS image and given essential sonar and imaging parameters, we have looked at several techniques to enhance the image for point scatterer detection, from purely magnitude-based image analysis to metrics involving the wavenumber domain to obtain various statistics in multilook images [10], and wavelet shrinking using the coherence of the wavelet decomposition of two multilook images inspired by [11]. The result of this step is an image with enhanced point scatterers and reduced speckle, which facilitates detection of candidate point scatterers.

For the detection step, we choose the pixel coordinates of a region of interest (ROI) centered around suitable local maxima in the enhanced image. Subsequently, for each detected point scatterer candidate, we extract several features from the measured PSF, with the most important being the measured along-track and across-track resolution. This is inspired by [8] who calculate the actual resolution from detected reflectors sorted by size. Additionally, we calculate features such as peak main lobe to average power level outside the main lobe and peak main lobe to peak transmission grating lobe level.

Finally, we convert the point scatterer features into a sharpness metric. We suggest that the ratio of the maximum (i.e., best) resolution to the measured resolution is equivalent to the ratio of the focused energy, F , to the total energy (focused

and defocused), F+D. We can then construct a resolution loss factor,

$$\alpha = \frac{F}{F + D} = \frac{\sigma_{max}}{\sigma_{measured}}. \quad (1)$$

The impact of resolution loss on the system performance, $\gamma_{resolution}(\alpha)$, can be estimated by running the system repeatedly on high resolution images while artificially imposing an increasing resolution loss. For the specific case of MCM where the target sizes are known, this factor can be scaled to reflect the minimum number of independent pixels per dimension on the target in order to obtain a certain detection and classification score [12], [13]. The degradation of resolution should be slowly varying over the image. In areas where we detect many candidate point scatterers, we expect the majority of their resolution estimates to be consistent, and can let the local median value represent the resolution of the area. For areas without candidate point scatterers, we could have noise or speckle, and neither can provide any information on the resolution.

Grating lobes degrade the image by generating defocused image replicas, mainly along the along-track axis [14]. A degradation is only observed where the grating lobe replica is strong compared to the local scatterers. Assuming that the energy from grating lobes, G , can be separated from the energy without grating lobes, S , we can construct a quality factor,

$$\gamma_{gratinglobe} = \frac{S}{S + G}. \quad (2)$$

The degradation from grating lobes is mainly local to along-track areas next to strong scatterers, and must be evaluated over the entire image with only local smoothing.

We may combine the different coherence contributions into a resulting image-based sharpness estimate,

$$\gamma_{sharpness_{image}} = \gamma_{resolution} \cdot \gamma_{grating}. \quad (3)$$

This estimate together with $\gamma_{sharpness_{meta}}$ results into a final sharpness estimate $\gamma_{sharpness}$, which in turn can be combined with the interferometric coherence, representing the signal-to-noise ratio, and theoretical geometric resolution as well as radiometric resolution into a final image quality metric as suggested in [2].

IV. RESULTS

Our starting point is a SAS image from the Oslofjord in Norway with flat seafloor obtained by FFI's HUGIN AUV equipped with interferometric two-sided HISAS 1032, see Fig. 2. Both the HUGIN AUV and HISAS are developed in cooperation of FFI and Kongsberg Maritime. The displayed scene features a larger rock outcrop on short range, rather featureless seafloor at medium range and some unknown strong scatterers at max range. The vehicle depth and height are around 40 m and 25 m respectively, hence deep enough to avoid any unwanted multiple reflections from the sea surface. The signal-to-noise ratio is high in the whole image covering a seafloor patch of 140 m \times 140 m. Meta-data predictions indicate neither vehicle crab nor deviation from a straight vehicle track

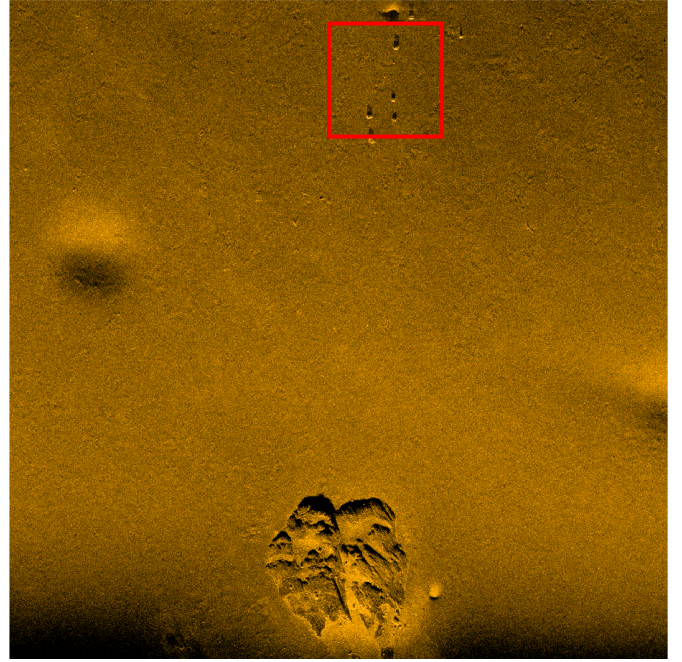


Fig. 2. Speckle-reduced SAS image of size 140 m \times 140 m with seafloor in the Oslofjord in Norway. Range increases from 30 m (bottom) to 170 m (top). The red rectangle marks the area from Fig. 4.

and micronavigation coherence is good as well. Everything points at that this image is of high quality and without any visible degradation.

To demonstrate our image-based sharpness estimation, we induce different types of common errors and re-run the SAS imaging processor to produce realistic, but degraded versions of the image from Fig. 2. The induced errors we focus further on are sound speed, yaw and surge, one at a time. In Fig. 3 we illustrate the influence of these three kinds of errors to the PSF for a simulated strong point scatterer at 60 m range. For each type of error we examine two realizations, resulting in a weaker and a stronger degradation. Key observations are:

- With increasing error in sound speed or surge scaling, the along-track resolution deteriorates strongly. Already for the smallest error the resolution changes from 2.8 cm to 6.4 cm and 5.1 cm, respectively. Interestingly, yaw error does not appear to have any impact on the resolution.
- Yaw error introduces grating lobes. The higher the yaw error, the higher the grating lobes. A larger surge error also introduces grating lobes, but not as strong as with yaw error.
- None of the induced errors have an impact on the across-track (range) resolution.

We have chosen to induce the following errors to the original data forming the SAS image from Fig. 2: 10 m/s added sound speed error, 0.2° added yaw error and 1.006 surge scaling error. These values are not unrealistic in practice and lie in between those shown in Fig. 3. The original image from Fig. 2 as well as the three degradations are shown more detailed in Fig. 4 for a chosen area of size 24 m \times 24 m

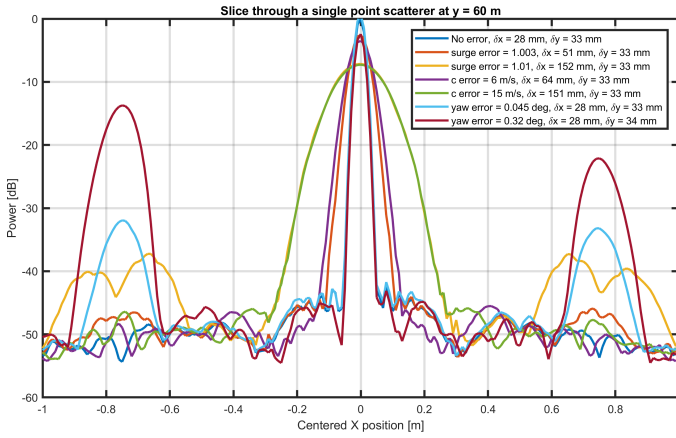


Fig. 3. Effects to point-spread function by errors in surge, sound speed and yaw.

at around 150 m range. Two different methods for image enhancement and detection were used to locate candidate point scatterers, shown in cyan circles and white diamonds. The first method (cyan) only operates on the magnitude images using a 2-D difference of Gaussians function, while the second method (white) uses a wavelet shrinking algorithm utilizing the coherence of wavelet coefficients over three scales for two independent looks obtained from the wavenumber domain.

Each type of induced error has a different effect on the final image. With sound speed error the image appears slightly more blurred and scatterers are range shifted from their original position. For 10 m/s increased sound speed, there is a shift of around 1 m at max range. Regarding yaw error, grating lobes are clearly visible as phantom echoes to the sides of the largest structures on the seafloor. The energy from the main object is distributed, hence the object echo appears weaker than in the original image, which also leads to less contrast between highlight and shadow. In the case of degradation due to surge error, we clearly see a blurred image. Scatterers are stretched along-track, hence deterioration in resolution. The scatterers may also be along-track shifted, dependent on the surge scaling error.

Concerning the two fundamentally different methods for detecting candidate point scatterers, we observe that they agree on some but far from all detections. Visually and due to the lack of ground truth information, each method's result seems plausible in most cases such that it is difficult to judge which method performs better. Both methods have the highest number of detections in the original image indicating that an image without degradation features more point scatterers. The image with surge error yields the lowest number of detections. Since each detection is performed independently from the original image or the other degradations and without any feature-matching, only some point scatterers are detected persistently in all images. This is not a problem as long as the chosen candidates are suitable for extracting features from the point-spread function and are scattered across the image, which appears to be true here.

Focusing on the complete images of size $140\text{ m} \times 140\text{ m}$, we extract a number of features in regions of size $30\text{ cm} \times 20\text{ cm}$ centered around each detection. In Fig. 5 we present the median along-track (a) and across-track (b) resolution versus range, smoothed in a moving average window of 10 m (for the wavelet-based set of detections, but results are comparable for the other set of detections). Theoretical resolutions for these images are 3.7 cm along-track and 3.2 m across-track. In the smoothed plots in Fig. 5, the lowest resolutions are around 4.9 cm along-track and 4.3 cm across-track, which is a good achievement for a set with real data. Across-track resolution is as expected close to constant for any of the images. Both the non-degraded and the yaw error image have comparable along-track resolutions independent of range. Sound speed error and surge error causes loss of along-track resolution with increasing range (as already indicated in Fig. 3) with the surge case being the worst in terms of along-track resolution (as can be observed by comparing the images of Fig. 4).

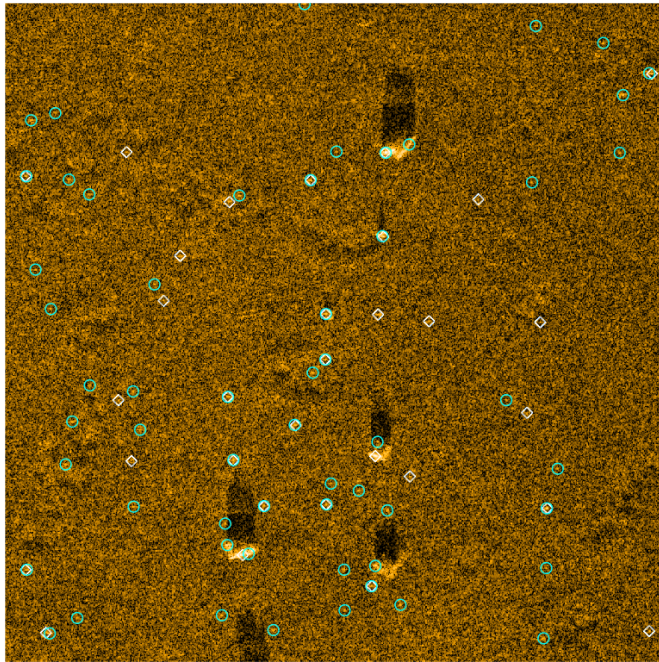
Grating lobes constitute shifted and defocused replica of the image. A resulting degradation mainly occurs where these replicas are strong compared to the local scene. The degradation from grating lobes is therefore local, and no direct range dependence as in Fig. 5 can be expected.

V. SUMMARY

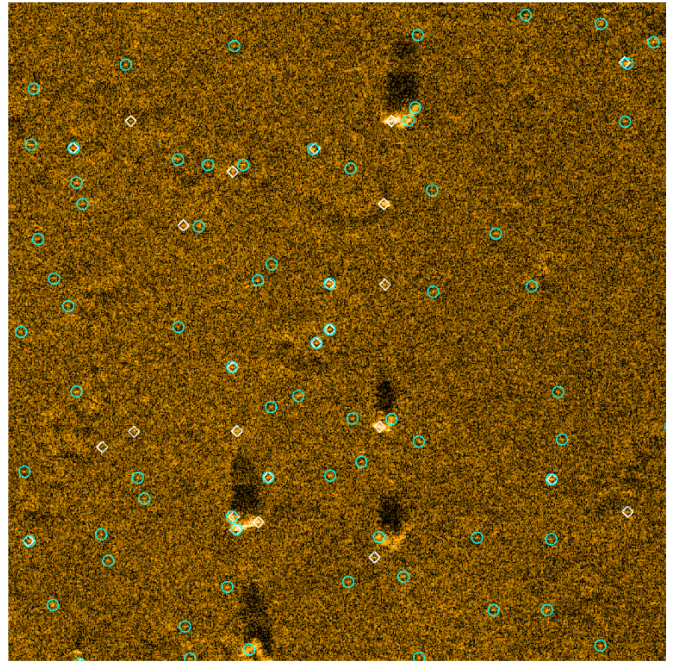
This work is a contribution to FFI's ongoing efforts to improve automated MCM. For the sonar mine search phase, the main inputs are through-the-sensor estimates of image quality and image complexity. The most important parameters for image quality estimation are the signal-to-noise ratio (derived reliably from interferometric coherence) and sharpness. Degradations of image quality due to e.g. noise or multipath are captured by the signal-to-noise ratio, while navigational errors, nonlinear vehicle tracks and sound speed errors are to be captured by the sharpness parameter. Previously, this one has been predicted by meta-data only. In this article we have described ideas how to additionally use information from the actual SAS images by locating suitable point scatterers and extracting features of their point spread function describing loss of image resolution and unwanted grating lobes. This approach requires texture in the image. If no point scatterers are detected (i.e. due to noise or speckle), sharpness will only be estimated from meta-data.

Utilizing through-the-sensor data becomes more important with an increasing degree of autonomy in modern AUV-based minehunting. The system needs to be able to validate collected sensor data itself. For instance, if the estimated sharpness, hence the quality of SAS images produced on-board during a mission, is not considered good enough, an alternative algorithm could be applied for re-imaging with the goal to provide the best possible data quality at the end of a mission.

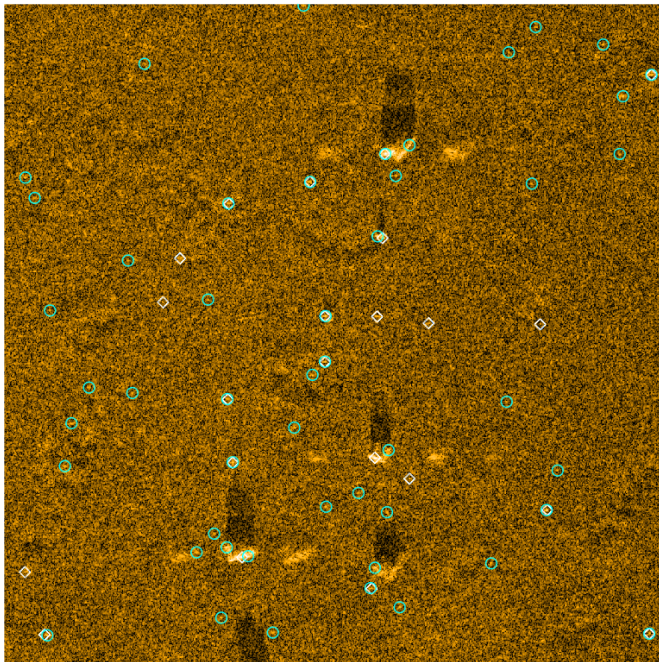
We have suggested a framework for through-the-sensor estimation of image sharpness. We have also investigated candidate methods for identification of point scatterers and extraction of attached image quality metrics. This is ongoing work, and it is unclear which method for feature extraction and



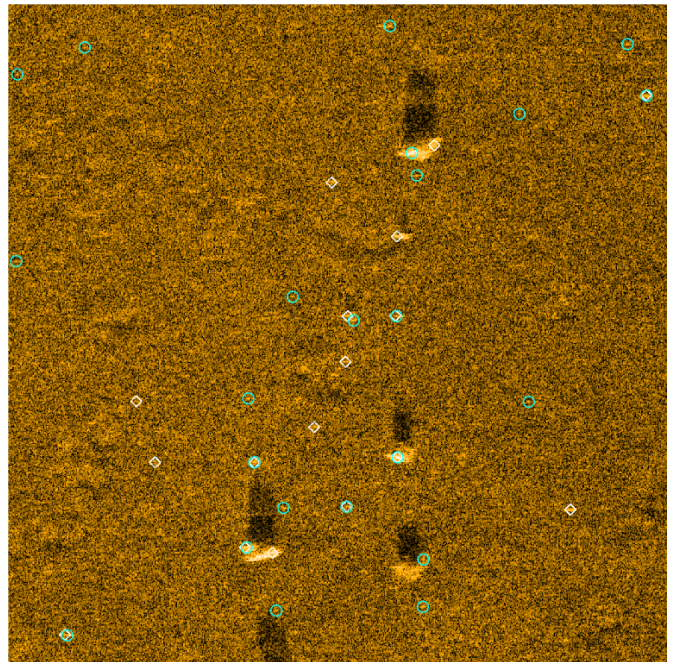
(a) Original non-degraded SAS image



(b) SAS image with induced 10 m/s sound speed error

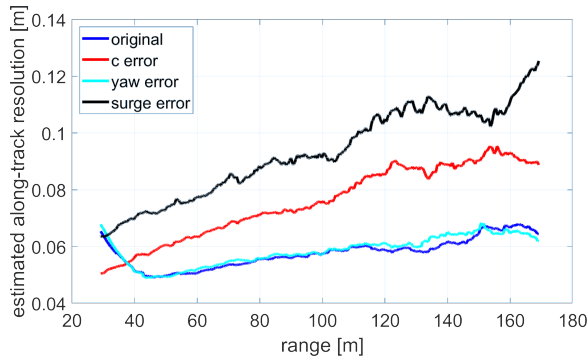


(c) SAS image with induced 0.2° yaw error

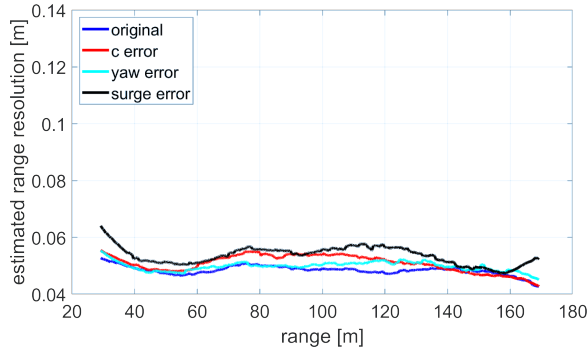


(d) SAS image with induced 1.006 surge scaling error

Fig. 4. Detailed area of the image from Fig. 2 (red rectangle) of size $24\text{ m} \times 24\text{ m}$ at around 150 m range with candidate point scatterers using two different enhancement and detection methods (white diamonds and cyan circles).



(a) Median along-track resolution



(b) Median across-track resolution

Fig. 5. Resolution versus range (moving average over 10 m range) for images with different degradations.

candidate point scatterer detection performs best. A thorough validation for robustness needs to be performed, both on simulated and real data examples of varying degradation and image texture level. Moreover, merging key point scatterer function features into a image-based sharpness estimate as well as constructing a final sharpness estimate including meta-data predictions have to be validated.

REFERENCES

- [1] Ø. Midtgaard, I. Alm, T. O. Sæbø, M. Geilhufe, and R. E. Hansen, "Performance Assessment Tool for AUV based Mine Hunting," in *SAS & SAR conference 2014, Proc. IOA*, vol. 36 Pt. 1, Lercici, Italy, September 2014, pp. 191–200.
- [2] R. E. Hansen and T. O. Sæbø, "Towards Automated Performance Assessment in Synthetic Aperture Sonar," in *Proc. Oceans 2013 MTS/IEEE*, Bergen, Norway, June 2013.
- [3] M. Geilhufe and Ø. Midtgaard, "Quantifying the complexity in sonar images for MCM performance estimation," in *Proc. 2nd UACE*, Rhodes, Greece, June 2014, pp. 1041–1048.
- [4] S. A. Synnes, R. E. Hansen, and T. O. Sæbø, "Assessment of shallow water performance using interferometric sonar coherence," in *Proceedings of Underwater Acoustic Measurements 2009*, Nafplion, Greece, June 2009.
- [5] D. Massonnet and J. Souyris, *Imaging with synthetic aperture radar*. EFPL Press, 2008.
- [6] D. A. Cook and D. C. Brown, "Synthetic aperture sonar image contrast prediction," *IEEE Journal of Oceanic Engineering*, vol. 43, no. 2, pp. 523–535, April 2018.
- [7] C. Oliver and S. Quegan, *Understanding Synthetic Aperture Radar Images*. Artech house, Inc., 1998.
- [8] N. Glover and I. Campbell, "Simultaneous low and high frequency high resolution SAS and a statistical method of quantifying the resolutions obtained," in *Proc. Inst. Acoust. Int. Conf. SAS/SAR*, vol. 32, no. 4, 2010, pp. 51–55.
- [9] R. E. Hansen, H. J. Callow, T. O. Sæbø, and S. A. Synnes, "Challenges in seafloor imaging and mapping with synthetic aperture sonar," *IEEE Transactions on Geoscience and Remote Sensing*, vol. 49, no. 10, pp. 3677–3687, 2011.
- [10] M. J. Sanjuan-Ferrer, I. Hajnsek, K. P. Papathanassiou, and A. Moreira, "A new detection algorithm for coherent scatterers in SAR data," *IEEE Transactions on Geoscience and Remote Sensing*, vol. 53, no. 11, pp. 6293–6307, November 2015.
- [11] A. J. Hunter and R. van Vossen, "Sonar target enhancement by shrinkage of incoherent wavelet coefficients," *The Journal of the Acoustical Society of America*, vol. 135, no. 1, pp. 262–268, 2014.
- [12] J. Johnson, "Analysis of image forming systems," in *Image intensifier symposium*. Fort Belvoir, VA: U.S. Army Engineer Research and Development Laboratories, 1958, pp. 249–273.
- [13] V. Myers and M. Pinto, "Bounding the performance of sidescan sonar automatic target recognition algorithms using information theory," *IET Radar Sonar Navig.*, vol. 1, no. 4, pp. 266–273, August 2007.
- [14] D. A. Cook and D. C. Brown, "Analysis of phase error effects on stripmap SAS," *IEEE Journal of Oceanic Engineering*, vol. 34, no. 3, pp. 250–261, July 2009.